MULTIPHOTON ION IMAGING:

A STUDY OF CHLORINE OXIDE

A Senior Scholars Thesis

by

CHRISTIAN DANIEL FREEMAN

Submitted to Honors and Undergraduate Research
Texas A&M University
in partial fulfillment of the requirements for the designation as

UNDERGRADUATE RESEARCH SCHOLAR

May 2012

Major: Physics
Mathematics

MULTIPHOTON ION IMAGING:

A STUDY OF CHLORINE OXIDE

A Senior Scholars Thesis

by

CHRISTIAN DANIEL FREEMAN

Submitted to Honors and Undergraduate Research
Texas A&M University
in partial fulfillment of the requirements for the designation as

UNDERGRADUATE RESEARCH SCHOLAR

Approved by:

Research Advisor: Simon North
Associate Director, Honors and Undergraduate Research: Duncan MacKenzie

May 2012

Major: Physics
Mathematics

ABSTRACT

Multiphoton Ion Imaging: A Study of Chlorine Oxide. (May 2012)

Christian Daniel Freeman
Department of Physics and Astronomy
Texas A&M University

Research Advisor: Dr. Simon North
Department of Chemistry

We present an analysis of the multiphoton excitation and ionization of the atmospheric radical chlorine oxide in the range 265-275nm using a molecular beam ion imaging apparatus. These experiments were motivated by previous work, as well as past unpublished results internal to our group. In sum, the resonance enhanced multiphoton ionization spectrum of chlorine oxide contains structure not easily explained by the known ionization pathways involving Rydberg states. An ion pair intermediate state was suggested to be the culprit behind the structured spectrum. In this work, we identify and characterize those ion pair intermediate states by analyzing spectra as well as using state selected velocimetry. Additionally, the nature of the ionization pathway allowed us to offer an estimate for rotational constants (B = .257 cm^{-1} and B = .195 cm^{-1}) of the previously identified ion pair intermediate states, as well as the vibrational constants (ω_e = 1110.9 cm^{-1} and $\omega_e\chi_e$ = 11.212 cm^{-1}) of the terminal chlorine oxide cation.

ACKNOWLEDGMENTS

I’d like to thank Dr. Simon North for his patience and enthusiasm throughout this project.

I’d also like to thank Michael Grubb for his constant aid throughout the course of the project, without which the project would not exist at all.

NOMENCLATURE

$REMPI$	Resonance Enhanced Multi-Photon Ionization
ClO	Chlorine Oxide

TABLE OF CONTENTS

LIST OF FIGURES

CHAPTER I

INTRODUCTION

This project aimed to fill in the details of some interesting results obtained by Cooper et. al in the late 1990s. We present a brief analysis of his team's results, as well as a sketch of our plan of attack.

The messy REMPI spectrum

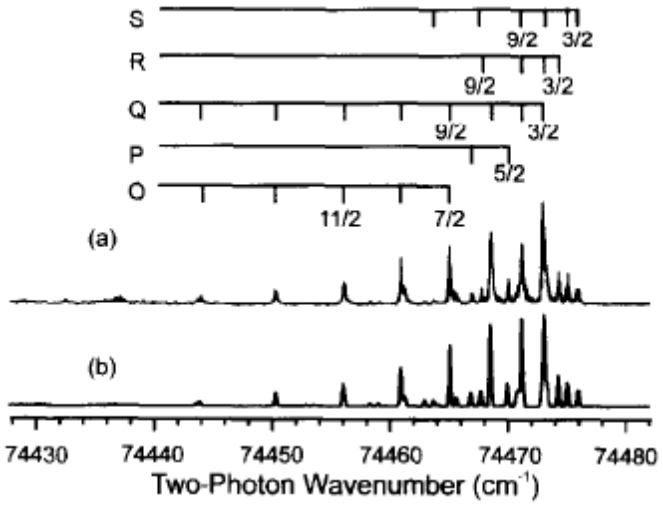

FIG. 1. Heavily zoomed in slice of the REMPI spectrum of ClO[1]. (a) depicts Cooper's experimental results, (b) depicts a simulation using a rotational temperature of 15K and a spectral linewidth of .2 cm^{-1}.

This thesis follows the style of *Journal of Chemical Physics.*

Cooper's team obtained their spectrum in Fig. 1 via (2+1) REMPI with a mass spectrometer. For the complete details see [1]. The structure is interesting, because it cannot be modeled via the known Rydberg, or highly excited states of ClO that lie in this region (the G and H states). The fit Cooper's team produced in Fig. 1 requires a much longer bond length (2.43Å), or 1.6 times that of the ground state. This is particularly telling, because by a back of the envelope calculation of simply summing the ionic radii of the fragments—i.e. Cl^+ and O^- (2.25 Å) or Cl^- and O^+ (2.03 Å)—suggests that maybe an ion pair state is responsible, at least partially, for the busy spectrum.

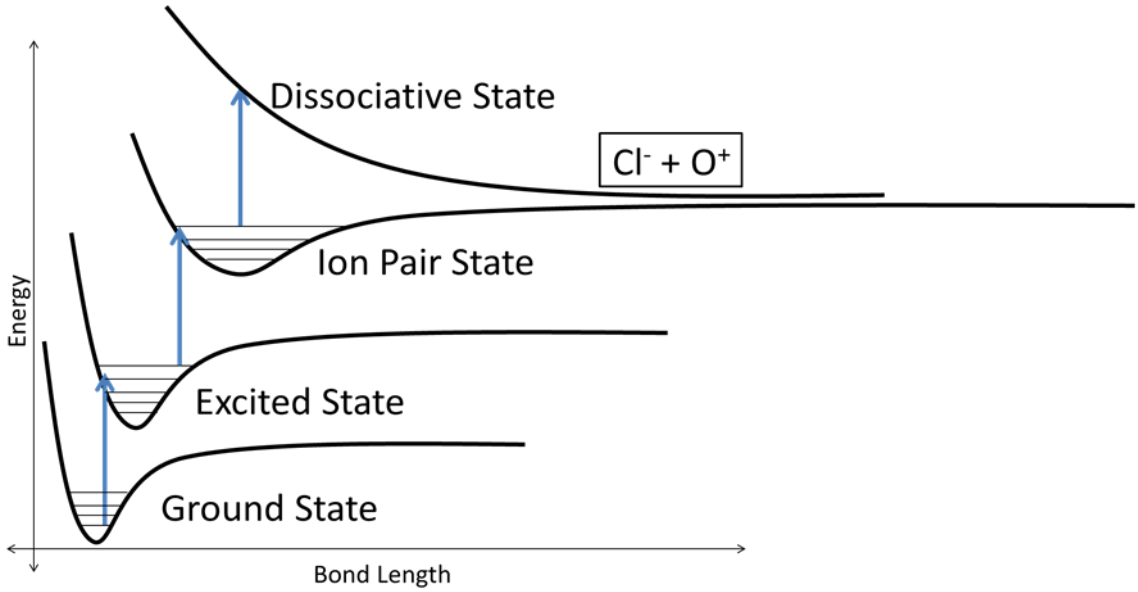

FIG. 2. Schematic diagram of Cooper's theory. The 3-photon photodissociation of ClO occurs via some ion pair intermediate state. Blue arrows indicate photon absorption and subsequent excitation between different potential energy surfaces. The ground state ($X^2\Pi$) and excited state ($A^2\Pi$) are well understood. The ion pair state and the precise dissociative states are not.

Cooper's theory has a handful of testable predictions. Chiefly, upon dissociating (the third step in Fig. 2), both a positively charged and negatively charged fragment should be produced.

Plan of attack

Our molecular beam ion imaging apparatus gives us the spectroscopic capabilities of Cooper's team, but also gives us additional information about the resultant atomic states after dissociation[2]. The extent to which these additional capabilities aid us will be made more precise in chapter 2, particularly in the context of Franck-Condon factors, which govern the relative probabilities of product channels in a transition. Most importantly, our detector offers us state sensitivity—we are sensitive to both how many different states of a given fragment are produced, and in what relative abundance. Preliminary investigations have not been able to reproduce *any* of the negatively charged fragments that Cooper's results predict, suggesting one of two things. First, there may exist a different pathway for the reaction through some previously unidentified Rydberg state, which would contradict the characteristically long bond length indentified by Cooper's team. Secondly, there may exist an additional step entirely after the ion pair state, which Cooper's team was not quite sensitive to. We will formalize our evidence for both the reality of the ion pair state and the reality of the additional step with our results in chapter 3. Further, our analysis in chapter 4 will ground this evidence.

CHAPTER II

METHODS

Experimental setup

The complete experimental setup is described in varying detail within [3] and [4]. Cl_2O was trapped using the methods of [5], and held at approximately $-75° \, C$ in a mixture of dry ice and acetone. To produce the ClO, we pulsed a mixture of Cl_2O and Helium through a pyrolitic source via a pulse valve. We ran a current of approximately 3 amps, which resistively heated the source, causing pyrolitic breakdown of the Cl_2O into ClO. The temperature of the source as a function of current was derived by a former group member, Hahkjoon Kim, and detailed in his thesis:

$$T = 160.49 * I + 196.85 \quad (1)$$

After passing through the source, the He/Cl_2O/ClO mixture was directed through a skimmer and collimated into a narrow beam. The beam then passed through the ion optics, where it was intersected by the laser (see fig. 3).

The fundamental output of a YAG laser (at 1064nm) was doubled to 532nm and then recombined with the fundamental to yield 355nm, essentially the third harmonic of the laser, in optical parlance. This light was directed through a dye cell containing a mixture of methanol and Coumarin 500 to produce wavelengths near 265nm. To reach wavelengths near 270nm and above, the dye mixture was changed to Coumarin 540 and methanol. We then optimized the laser output to yield roughly 150 to 200 μJ per shot.

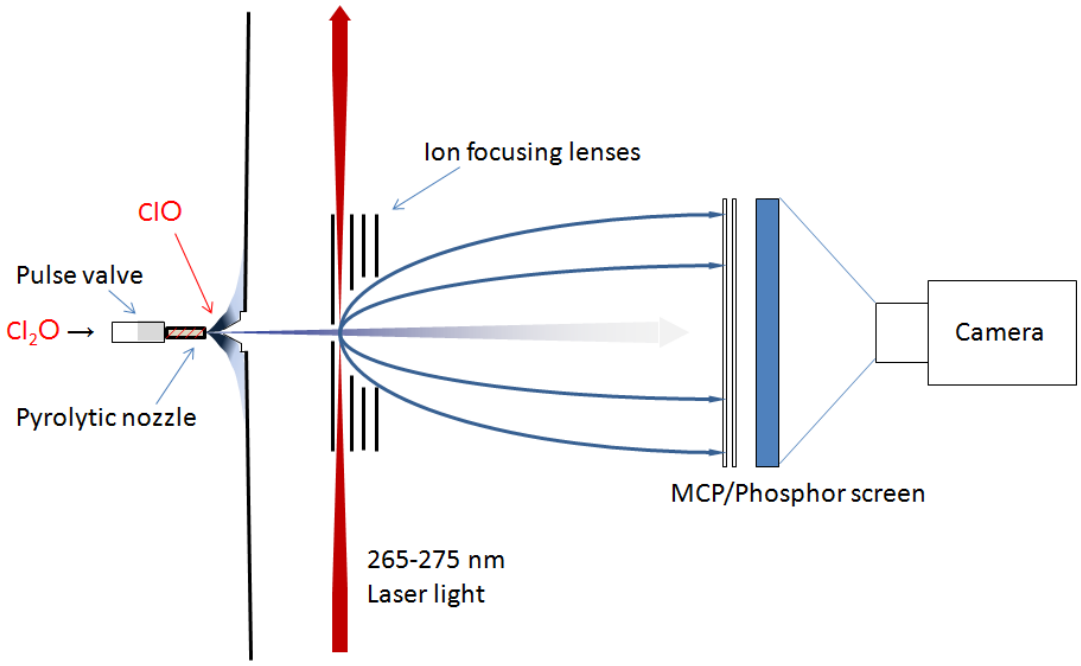

FIG. 3. Schematic diagram of our experiment. ClO mixture is skimmed and directed through chamber. Laser light dissociates the ClO, which breaks apart into chlorine and oxygen fragments, indicated by the blue curves. These fragments accelerate down the 50cm long time of flight tube via the electric field generated by the ion optics and strike the detector.

Because any ion striking the MCP/Phosphor screen will cause visible fluorescence, we gate the camera to only record at specific intervals synchronized with the intervals of the pulse valve firing, but offset so as to allow time for ions of the desired mass to reach the detector, schematically represented in Fig. 3. For the ion focusing lenses held at 3000 V, 2658 V, and 2310 V, we used the experimentally determined formula:

$$t_{offset} = .8912 * \sqrt{mass} + .013 \quad (2)$$

This formula supplies the offset to use to record ions of a given mass striking the detector. As an example, by using 16 for the mass (in AMU), we could calculate the offset to see Oxygen ions. Fig. 4 shows a to-scale view.

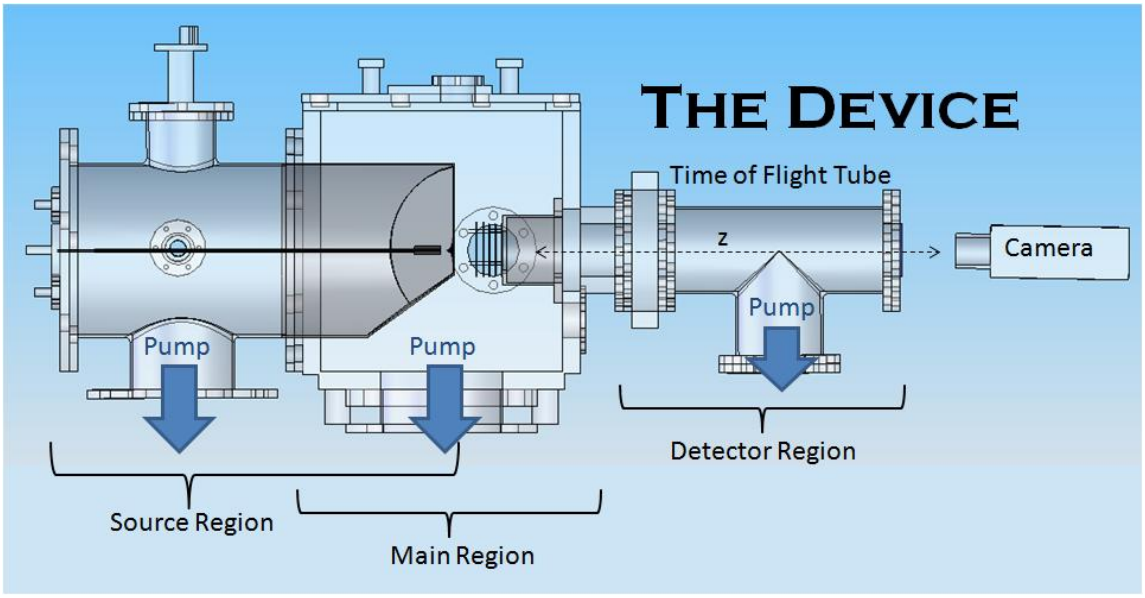

FIG. 4. Cutaway view of detector apparatus from Solidworks schematic. Chambers are held under high vacuum to prevent the MCP/Phosphor screen from being overwhelmed with signal.

Theory of ion imaging

When laser light strikes a ClO molecule and causes it to break apart, energy conservation requires:

$$E_{photon} - E_{bond} = E_{Cl\ internal} + E_{Cl\ kinetic} + E_{O\ internal} + E_{O\ kinetic} \tag{3}$$

To wit, the energy in the photon left over from the breaking the bond is apportioned between the kinetic and internal energy of the fragments. Momentum conservation tells us in what relative magnitude the kinetic energies of the fragments split:

$$m_{Cl}v_{Cl} = m_O v_O \Rightarrow \frac{1}{2}m_{Cl}v_{Cl}^2 = \frac{1}{2}\left(\frac{m_O m_{cl}}{m_{Cl}^2}\right)m_O v_O^2 \tag{4}$$

That is, if we can measure the velocity of one of the fragments, we can determine the velocity and kinetic energy of the other. By quantum mechanics, we know that the possible internal energies of the fragments exist at specific, known, quantized values.

In our experiment, the laser intersects the molecular beam at a right angle. Any given molecule of ClO will photodissociate with a probability given by the overlap, or dot product of the ClO bond axis vector with the polarization vector of the laser. As the molecules are oriented in all directions, and the laser is polarized either vertically or horizontally with respect to the beam, ClO molecules dissociate in all directions, but with an intensity governed by a $\cos^2\theta$ distribution, barring anisotropic effects. Depending on the type of dissociation, the orientation of that distribution can change, and other more complicated effects can smear the distribution out. For this experiment, however, we are chiefly concerned with the relative magnitudes and spacings of the rings. The expanding sphere of dissociated ions accelerates down the chamber and hits the detector, producing an image like in Fig. 5.

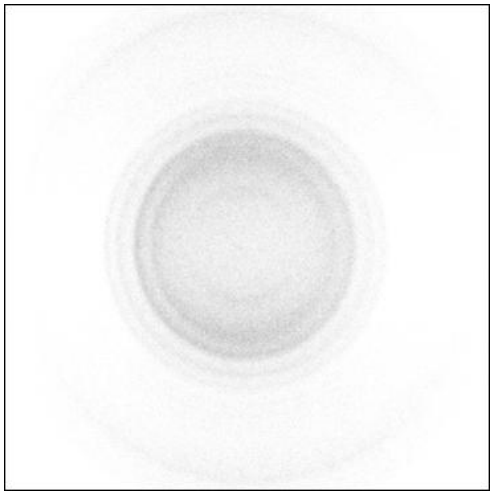

FIG. 5. Sample image depicting rings of oxygen ions. Signal has been integrated over several thousand shots with the MiPANTS technology suite.

By measuring the radii of the rings in pixels, we can perform a simple conversion from pixels to meters, or pixels to velocity. This so called speed to pixel ratio was

experimentally determined for our set of ion optics by comparing our data to a past, published experiment[6] from previous group members, and ends up being approximately 15.5 meters per second for every pixel from the "center" of the image. Centering the image was done via dynamically folding all quartiles of the image onto one another about some variable "center", and varying this center point until the quartiles overlapped. This functionality is available in MiPANTS. This introduces an error of ± 1 pixel in determining the center, so we do not expect to be able to fit the distributions better than by approximately 15 meters per second from centering alone. With the center known, and the speed to pixel conversion factor calculated, we can express our raw image intensity as a function of velocity using the RadPANTS technology suite developed by Michael Grubb and repurposed by myself, seen in Fig. 6.

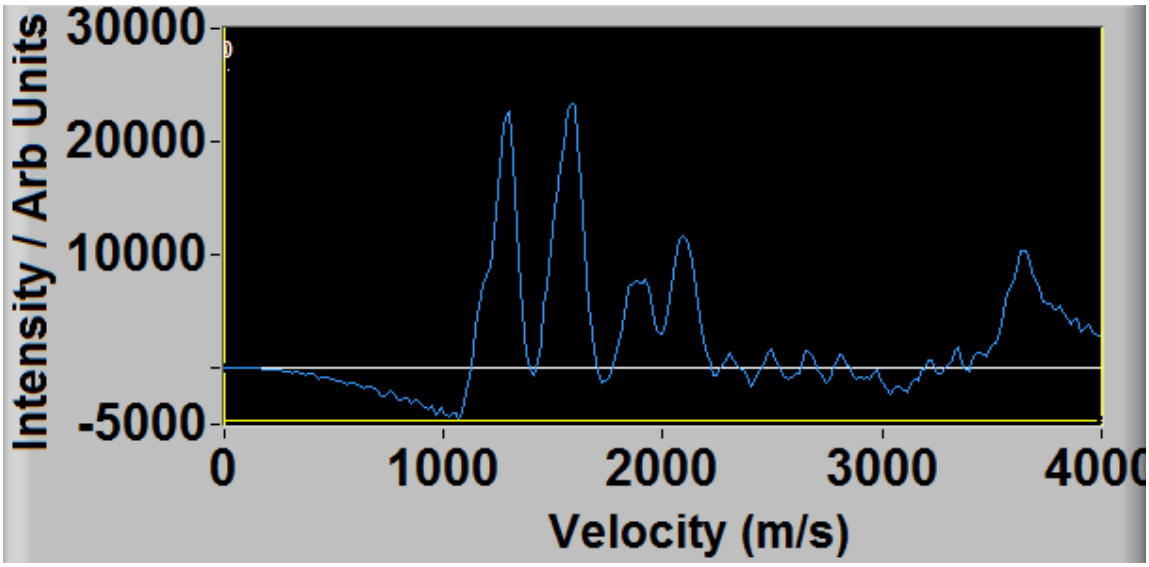

FIG. 6. Sample radial distribution. Signal is integrated at different radii about the center to determine the peaks in this image. The negative intensities were due to an error that was fixed.

We can directly read off the velocities of the fragments from this image. By equation (3), we know the photon energy, the bond energy, and now the kinetic energy, thus the structure of the peaks in this image corresponds to the different internal energies of the fragments responsible for each peak. As we will discuss in Chapter Four, the structure in this image is highly suggestive of a vibrational distribution, so RadPANTS has the additional functionality of overlaying a theoretical vibrational distribution, as in Fig. 7.

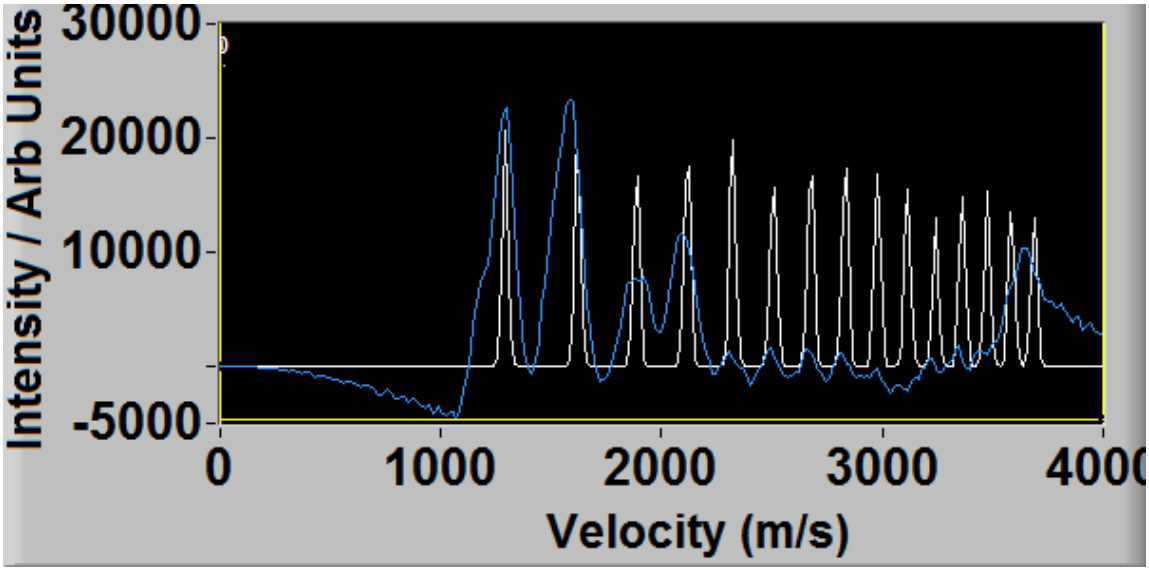

FIG. 7. Radial distribution from Fig. 6 with an overlaid theoretical vibrational distribution. Height of the peaks is set by the user. See Franck-Condon section for more discussion.

This vibrational spectrum can be determined three ways with RadPANTS. Firstly, it can be tuned by adjusting the vibrational constant and the anharmonicity constant by hand. Secondly, the user can input the locations of the peaks and the program will list fitting distributions via least squares analysis. Lastly, the user can set a threshold peak value and have RadPANTS perform automatic peak detection and list fitting constants via least squares analysis. Because of the huge amount of nonuniqueness in the problem, to

be discussed in Chapter Four, the hand tuning of peaks proved to be the easiest way to find best candidate fits.

The Franck Condon Principle

We would also like to be able to speak meaningfully about the relative intensities of the peaks in our radial distribution. For this we will need the Franck Condon Principle. From quantum mechanics, we can always express the probability of an electric dipole transition occurring as:

$$Probability\ of\ transition = \langle \psi' | \boldsymbol{\mu} | \psi \rangle \tag{5}$$

Where $\boldsymbol{\mu}$ is the electric dipole operator. If we expand $\boldsymbol{\mu}$ into electric and nuclear components, and we expand ψ into electronic, vibrational, and spin components, we have:

$$P = \langle \psi_e' \psi_v' \psi_s' | \boldsymbol{\mu}_e + \boldsymbol{\mu}_N | \psi_e \psi_v \psi_s \rangle \tag{6}$$

Within the Condon approximation, the electronic and vibrational wavefunctions are separable. Furthermore, within Born Oppenheimer approximation, the electronic component of the dipole operator only operates on the electronic wavefunctions, and the nuclear component of the dipole operator only operates on the vibrational wavefunctions. Because the electronic states are orthogonal, the nuclear terms disappear, and we are left with[7]:

$$P = \boxed{\langle \psi_v' | \psi_v \rangle} \langle \psi_e' | \boldsymbol{\mu}_e | \psi_e \rangle \langle \psi_s' | \psi_s \rangle \tag{7}$$

The boxed term is the Franck Condon factor. Essentially, the probability of the transition is governed by the overlap integral of the two vibrational states involved in the interaction.

Thus, if we think we know what vibrational states we have in our radial distribution, and if we think we know from which vibrational state those states came, we should be able to reproduce the relative intensities of the states. Given enough information about the potential surfaces involved in our interaction, these tools can allow us to completely characterize the vibrational spectrum in the regions we examined.

CHAPTER III

RESULTS

Preliminary comments

After we were unable to find the negative ion suggested by Cooper's team's theory, we decided to perform a mass-selected REMPI spectrum of the oxygen ion and chlorine ion signals over a range of wavelengths. After spotting a spike in our total signal at a mass corresponding to that of the chlorine oxide cation, we also recorded the REMPI spectrum for ClO+ over the range, shown in Fig. 8.

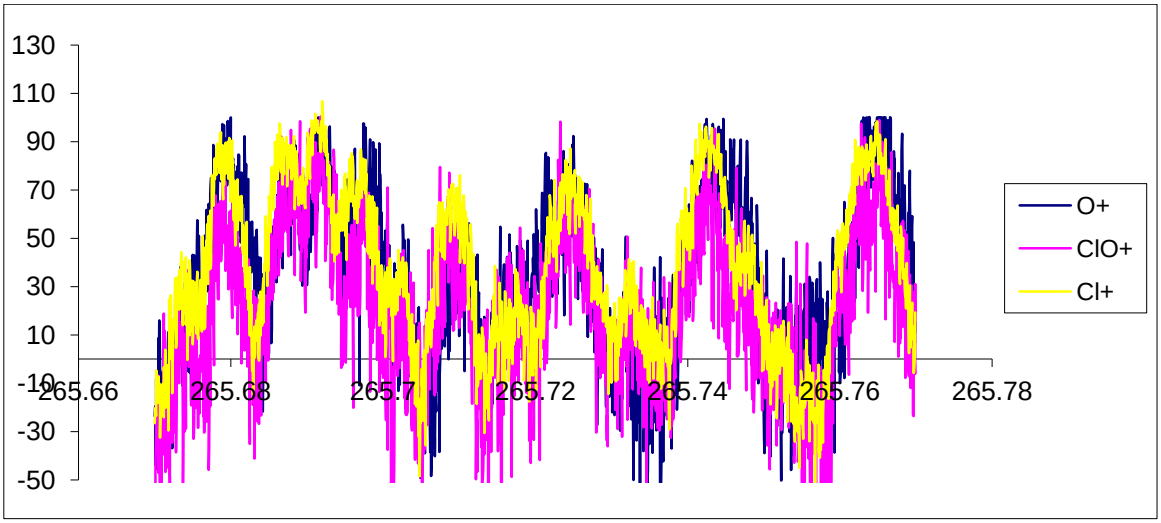

FIG. 8. Patch of REMPI spectra for O+, Cl+, and ClO+ for the range 268.5nm to 268.6nm.

We first observed that the O+ and Cl+ signals seemed to track each other—that is, the peaks in the REMPI spectrum of one exactly corresponded to peaks in the other. With no negative ions, the ion pair potential could not account for this correlated structure alone. That the ClO+ signal *also* tracked both the Cl+ and O+ signals, and that ClO+

lies approximately one photon in energy higher than the ion pair potentials was hugely suggestive. This tracking behavior occurred throughout the range of wavelengths we studied (approximately 263nm to 275nm). Chapter four will look at the structures present in the overall spectra more closely, in the context of rotational constants.

With this in mind, we postulated a new photodissociation pathway, depicted in Fig. 9.

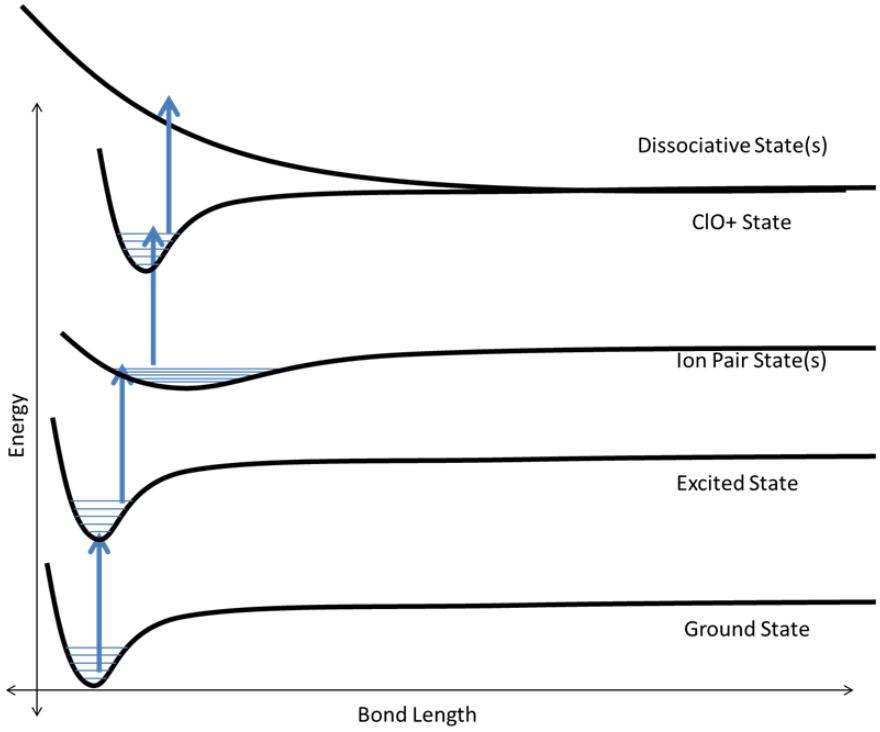

FIG. 9. Schematic augmented pathway (as compared to Fig. 2). An additional step from the ion pair state to the cation has been added before dissociation.

The third step in the above pathway requires an electron to be ejected from the ClO atom. The only "selection rule" governing the allowed kinetic energies that electron can take away (upon being ejected) amounts to requiring it follow:

$$E_{photon} + E_{ClO\ ion\ pair\ internal} = E_{ClO+\ internal} + E_{Electron\ kinetic} \quad (8)$$

Where this is just energy conservation applied to the third step in Fig. 9. The internal states of ClO+ are quantized vibrational states. Thus the third step can, in principle, populate every vibrational state of ClO+ below the threshold energy defined by the left hand side of equation 8 and above the ground state energy of ClO+. The relative magnitudes of the different vibrational states populated in this way are determined by the Franck-Condon factors between the ion pair state and the cation state. These Franck-Condon overlap factors will be discussed further in Chapter four.

Raw results

The bulk of the data was not REMPI spectra, but images like that of Fig. 5. To get a feel for the dynamics in this messy region, we looked at O+ and Cl+ images throughout in areas that had prominent peaks on the REMPI, as those areas corresponded to the most potential signal. These images are a selection of some of the best O+ accumulations:

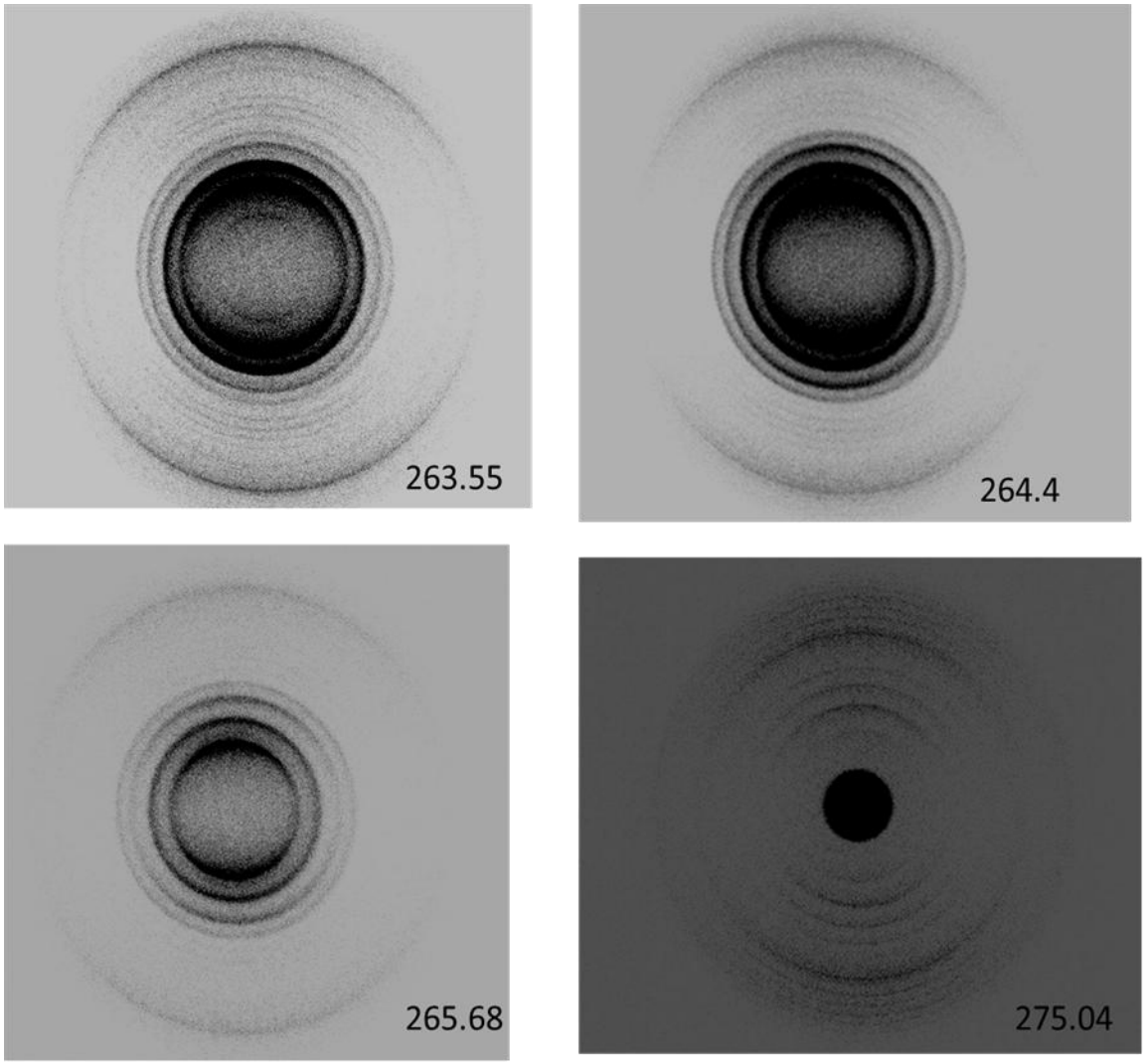

FIG. 10. Artificially darkened experiment images with 1-photon laser wavelength indicated. Each image is mass-gated for O+.

Again, each of the images in Fig. 10 corresponds to some peak on the REMPI spectra. Further, we suggest that each ring corresponds to an oxygen atom that originated from some individual internal state of ClO+. Because the vibrational spacing for the Cl+ images is so much closer, the ring structures visible are not nearly as compelling as these in Fig. 10. The prominent features for analysis in chapter 4 are the relative intensities,

spacings, and anisotropy within each of these images. Plotting the radial distribution—that is, the signal intensity as a function of radius, is even more suggestive of the vibrational structure, as seen in Fig. 11 and Fig. 12.

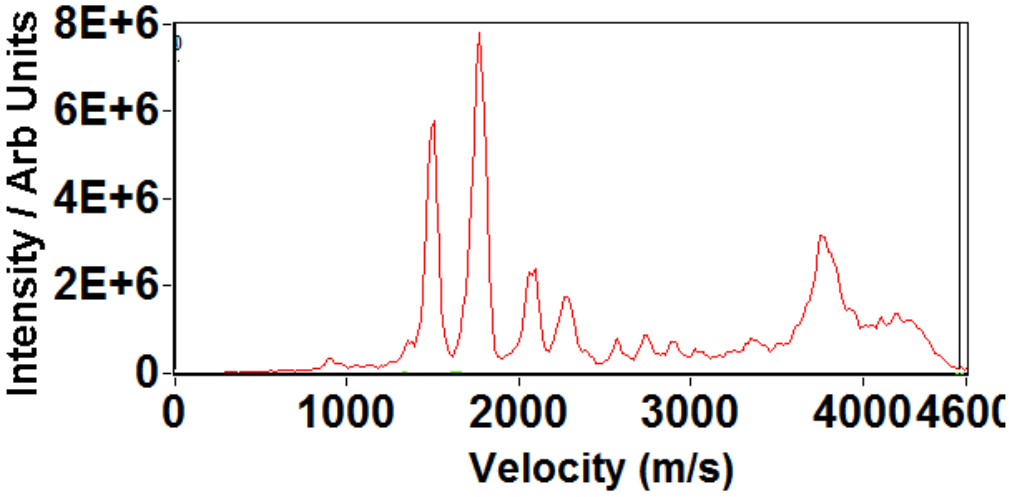

FIG. 11. O+ radial distribution for 263.55nm light.

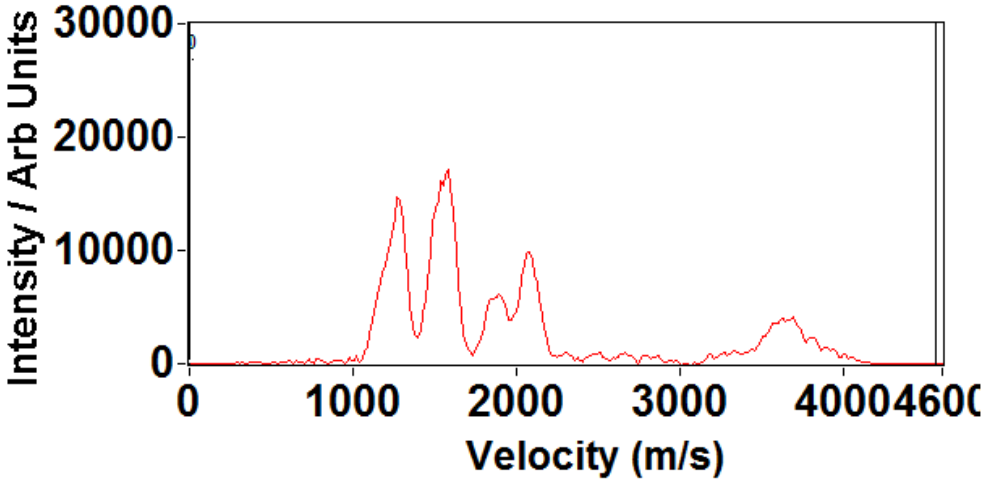

FIG. 12. O+ radial distribution for 265.39nm light.

Issues and further comments

Besides the general difficulty in synthesizing Cl_2O, and orneriness of the apparatus itself, the actual analysis of images was stalled for several weeks due to the lack of an accurate speed to pixel ratio. Besides that, once the speed to pixel ratio was known, analysis was nearly instantaneous, resulting in calculated vibrational constants that described that data. The radial distributions above in Figs. 11 and 12, particularly 12, exhibit the main difficulty in the analysis to be shown in chapter four. The "shoulders" present in the peaks of Fig. 12 are real, suggesting more than one pathway to the end products shown. This extra pathway could insinuate itself through either multiple intermediate ion pair states, multiple terminal cation states, or even multiple product channels. To level our analysis, we collaborated with Dr. Ian Lane at Queen's University Belfast, who was kind enough to perform some theoretical calculations for us.

We were quite certain of the final vibrational states in our images shown above. To be able to perform the Franck-Condon analysis, however, we needed to be sure about which vibrational state of the *ion pair* state we started from. As a cross check of our analysis, Dr. Lane provided theoretical calculations of the ClO+ lowest lying potentials, shown in Fig. 13.

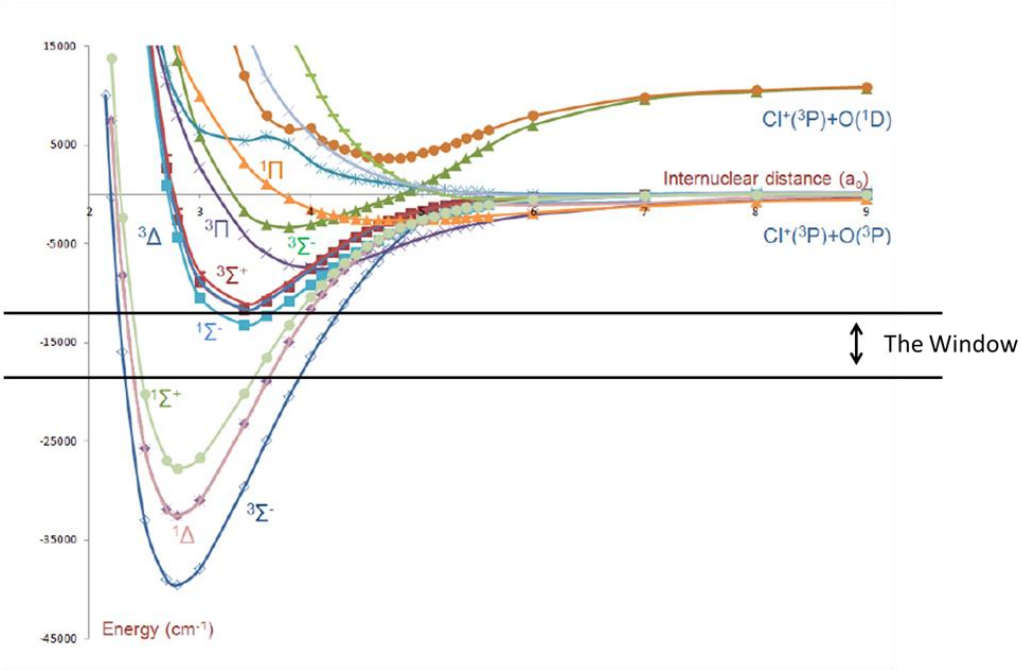

FIG. 13. Dr. Ian Lane's calculated lowest lying ClO+ potentials with asymptotes. The "window" indicated roughly corresponds to the range of energies the third photon could reach for the different laser wavelengths we used.

Thankfully, only the lowest lying of these states seems to contribute to the structure we see. To help us be able to perform the Franck-Condon calculation, Dr. Lane also calculated the lowest lying ion pair potentials:

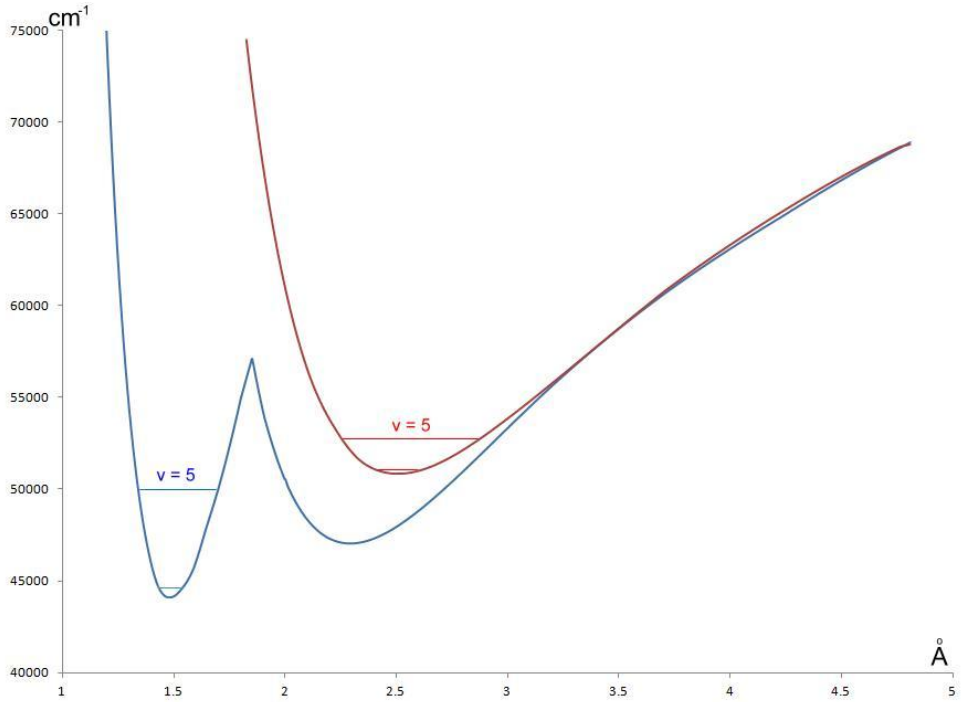

FIG. 14. Dr. Ian Lane's calculated lowest lying ion pair potentials with ground and fifth vibrational levels indicated on each. The tighter half of the blue potential is actually the Rydberg E state of ClO+, exhibiting a conical intersection with the lowest lying ion pair state.

For these two states in Fig. 14, we are probably accessing the higher energy state moreso than the lower, but this depends on the particular region of the spectrum we are probing, as the Franck-Condon factors for each potential differ.

Lastly, as a general difficulty, the spacing of the peaks for the radial distributions like those of Figs. 11 and 12 is on the order of 800 cm^{-1}—the difference in energy between the ground state chlorine atom and its first excited state. This makes it difficult to be able to distinguish between the O+ and Cl channel versus the O+ and Cl* channel. Furthermore, the two common isotopes of chlorine are in close enough abundance so as

to blur the signal intensities for our Cl+ images, but not so much as to make analysis impossible.

CHAPTER IV

ANALYSIS AND CONCLUSIONS

We will now formalize all of the evidence for the existence of the ion pair state, as well as motivate our interpretation of the peak spacings as representing the vibrational spacing of the ClO cation. If we isolate a band on the REMPI spectrum, like from Fig. 8, we can fit a rotational distribution to this band, shown in Fig. 15.

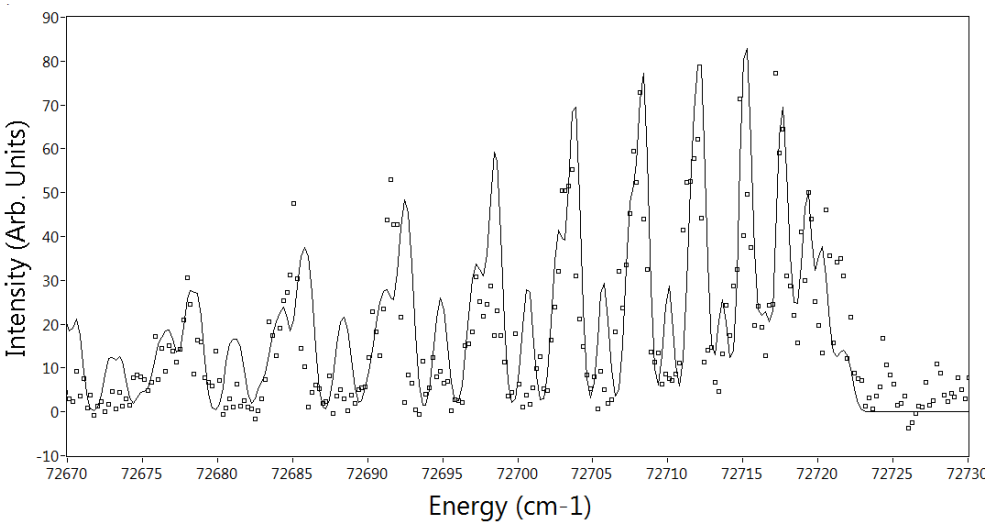

FIG. 15. Rotational distribution fit. The two-photon energy in wavenumbers is listed along the x-axis. The bond length arising from the spectroscopic constants is quite long. The pertinent constants are: T = 72720.2 cm^{-1}, B=.257 cm^{-1}, and r = 2.43 Å.

We see these bands across the entire wavelength range we probed.

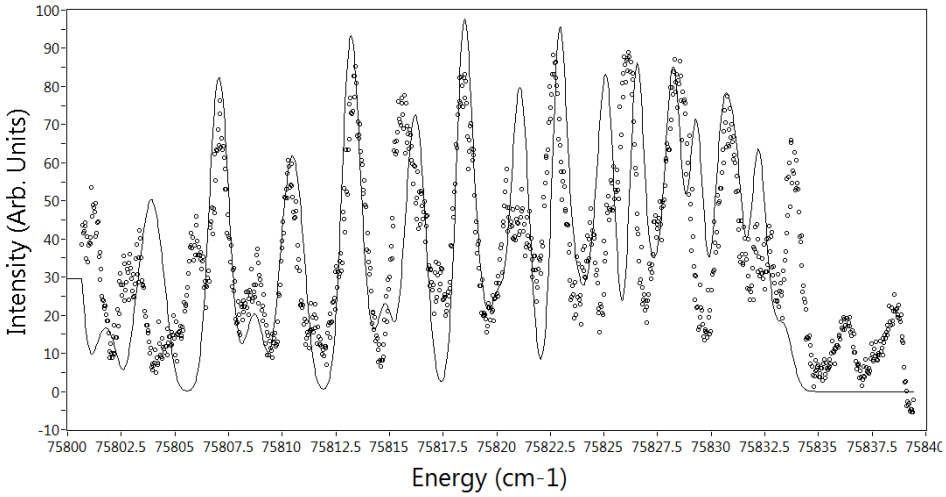

FIG. 16. Another rotational distribution fit. Again, the bond length is large, but even larger than the previous band. As our photon energy increases, it is likely we are accessing two different ion pair states. The pertinent constants are: T = 75832.3 cm^{-1}, B=.195 cm^{-1}, and r = 2.8 Å.

Theoretical calculations of the available ion pair states are ongoing, but these results are consistent with what we have been given so far. While Fig. 15 and Fig. 16 are instructive, to learn more about the ion pair states, we would need to perform a far more exhaustive REMPI analysis probably with a much more sensitive instrument. These results, however, are enough of a smoking gun to justify the second step of the process in Fig. 9.

We have to be more delicate with the treatment of the third step. Within our interpretation, the third photon ejects an electron of some kinetic energy, but brings the chlorine oxide to some excited state—in principle any of the three lowest lying excited states from Dr. Lanes theoretical picture in Fig. 13. The data are most consistent with that third photon *mostly* populating the ground state. Assuming this is true, we can

assign a "vibrational number" to each unique ring we see in any given number, as all the oxygen atoms in any given ring all came from the same vibrational state of ClO+. If that assignment is correct, then the radius of our observed rings actually gives an estimate of the vibrational energy of that assigned state.

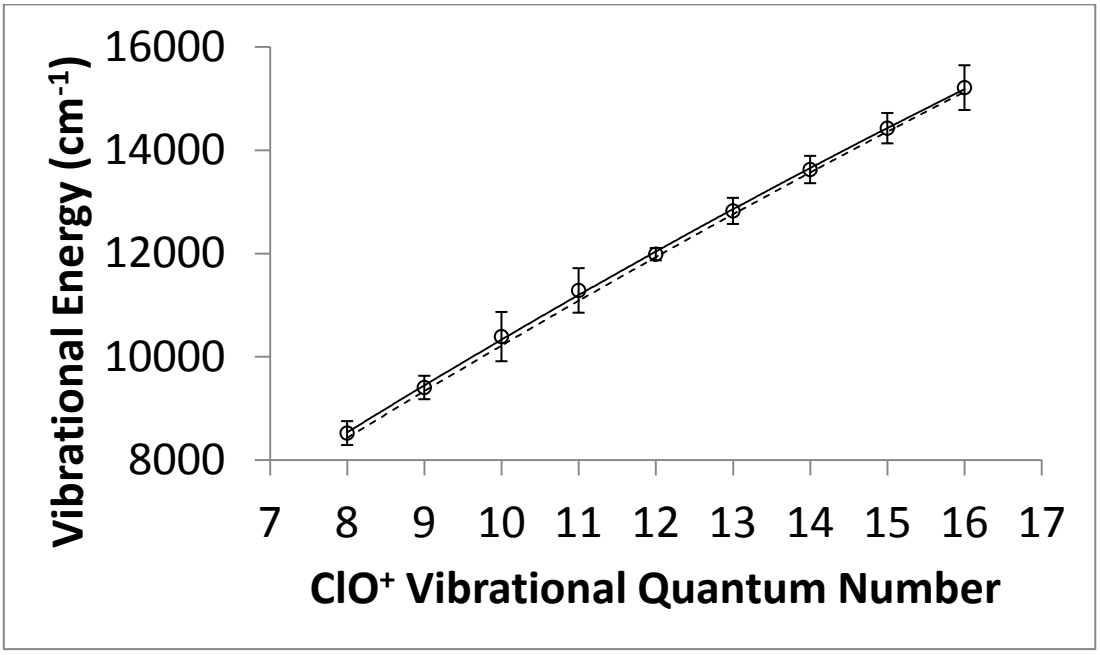

FIG. 17. Combined dataset. Dotted line is Dr. Ian Lane's theoretical calculation of the vibrational energy spacing. Circles with error bars are from approximately 5 combined images—some images only give estimates for the lower vibrational levels, some gave estimates to the higher levels.

Within the interpretation, the data in Fig.17 matches the simulation quite well. Our experiment data suggest an ω_e of 1110.9 cm^{-1}, and an $\omega_e\chi_e$ of 11.212 cm^{-1}. The theoretical fit yields similarly values with $\omega_{e\ theory}$ of 1073.4 cm^{-1} and $\omega_e\chi_{e\ theory}$ of 9.432 cm^{-1}.

In summary, we were able to estimate rotational constants for ion pair intermediate states, as well as vibrational constants for the ClO cation ground state. Ongoing analysis, aided by Dr. Ian Lane's calculation of theoretical potentials may aid us in backing out meaningful information via Franck Condon analysis. For future work, coupling that analysis with analysis of the anisotropies of the different rings could help pin down the exact exit channels.

REFERENCES

[1] M. J. Cooper, T. Diez-Rojo, L. J. Rogers, C. M. Western, M. N. R. Ashfold, J. W. Hudgens, Chem. Phys. Letters **272**, 232-238 (1997).

[2] M. P. Grubb, M. L. Warter, C. D. Freeman, N. A. West, K. M. Usakoski, K. M. Johnson, J. A. Bartz, S. W. North, J. Chem Phys. **135**, 094201 (2011).

[3] K. S. Dooley, M. P. Grubb, J. Geidosch, M. A. van Beek, G. C. Groenenboom, S. W. North, Phys. Chem. Chem. Phys. **11**, 4770 (2009).

[4] H. Kim, J. Park, T. C. Niday, S. W. North, J. Chem. Phys. **123**, 174303 (2005).

[5] E. Wiberg, N. Wiberg, A. F. Holleman, in *Inorganic Chemistry*, edited by N. Wibger and B. J. Aylett (Academic Press, San Diego, California, 2001), pg. 459

[6] H. Kim, K. S. Dooley, E. R. Johnson, S. W. North, J. Chem. Phys. **124**, 134304 (2006).

[7] A. S. Coolidge, H. M. James, R. D. Present, J. Chem. Phys. **4**, 193 (1936).

CONTACT INFORMATION

Name:	Christian Daniel Freeman
Professional Address:	c/o Dr. Simon W. North Department of Chemistry CHEM 2104 Texas A&M University College Station, TX 77843
Email Address:	daniel_freeman1990@yahoo.com
Education:	B.S., Physics, Texas A&M University, May 2012 B.S., Mathematics, Texas A&M University, May 2012 Magna Cum Laude Undergraduate Research Scholar